

ProactivePIM: Accelerating Weight-Sharing Embedding Layer with PIM for Scalable Recommendation System

Youngsuk Kim
Seoul National University
Seoul, Korea
youngsuk95@capp.snu.ac.kr

Junghwan Lim
Seoul National University
Seoul, Korea
jhljm@capp.snu.ac.kr

Hyuk-Jae Lee
Seoul National University
Seoul, Korea
hjlee@capp.snu.ac.kr

Chae Eun Rhee
Hanyang University
Seoul, Korea
crhee@hanyang.ac.kr

Abstract—The model size growth of personalized recommendation systems poses new challenges for inference. Weight-sharing algorithms have been proposed for size reduction, but they increase memory access. Recent advancements in processing-in-memory (PIM) enhanced the model throughput by exploiting memory parallelism, but such algorithms introduce massive CPU-PIM communication into prior PIM systems. We propose ProactivePIM, a PIM system for weight-sharing recommendation system acceleration. ProactivePIM integrates a cache within the PIM with a prefetching scheme to leverage a unique locality of the algorithm and eliminate communication overhead through a subtable mapping strategy. ProactivePIM achieves a 4.8× speedup compared to prior works.

I. INTRODUCTION

Deep learning-based personalized recommendation system serves as a pivotal technology in various companies [2], [19], [26], with the Deep Learning Recommendation System (DLRM) being a representative model. These systems account for a significant computational workload of data centers [8]. Figure 1 (a) shows the DLRM architecture, where dense features (user information) are processed through a bottom multi-layer perceptron (MLP), and sparse features (items) are handled by the embedding layer. The embedding layer performs gather-and-reduce (GnR) operations, which retrieve embedding vectors for items and perform element-wise addition. The outputs undergo feature interaction and top MLP, which generates Click-Through-Rate (CTR) as a result.

As depicted in Figure 1 (b), the memory-intensive nature of the embedding layer grows continuously, placing constraints on data center infrastructures [32]. Recent studies leveraged near-memory processing (NMP) and processing-in-memory (PIM) to accelerate AI models by exploiting memory parallelism [9], [12], [13], [14], [21]. For recommendation systems, TensorDIMM [13], RecNMP [12], TRiM [22] and SPACE [11] accelerated GnR via NMP and PIM to address memory-intensive characteristic. On the other hand, as shown in Figure 1 (b), the model size of DLRM has grown by 16 times from 2020 to 2024, as incorporating more items result in better model quality [17], [24]. Serving inference with a multi-node server or introducing solid-state drives (SSDs) could be solutions, but they produce high synchronization costs,

vulnerability to failures, and a negative impact on execution time [1], [33]. An algorithmic approach, the hashing trick [28], fits the model into the memory capacity budget at the cost of accuracy degradation. Weight-sharing algorithms, which transform the original embedding table into multiple small subtables, are proposed to compensate for such drawbacks. Nevertheless, these methods amplify the off-chip memory access and are still memory-intensive. Prior NMP/PIM systems for recommendation models are ineffective because the multiplication used in these algorithms requires operands from subtables to reside in the same NMP/PIM unit, unlike simpler GnR. This limitation necessitates CPU-PIM communication, causing severe overhead. Furthermore, they are not optimized for exploiting data locality of these methods. There exist other algorithmic methods [6], [16], but the weight-sharing algorithm is superior in degree of compression.

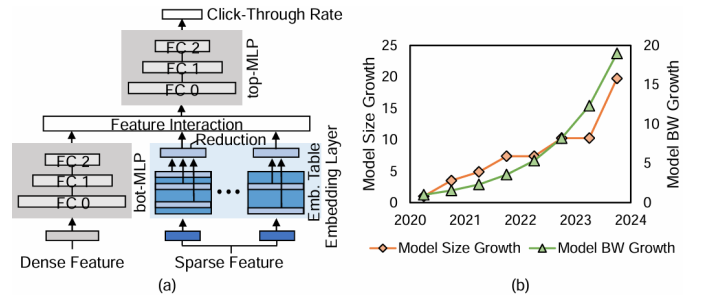


Fig. 1: DLRM overview (a) DLRM architecture (b) Model size and bandwidth growth. (Reproduced from MTIA [5] and RecShard [24])

We propose ProactivePIM, a PIM-integrated memory architecture to address data locality and CPU-PIM communication of weight-sharing algorithm inference. ProactivePIM is built on a heterogeneous DIMM-HBM system, where a 2-level PIM system is built within the HBM: base-die PIM (bd-PIM) and bank-group PIM (bg-PIM). We analyze weight-sharing algorithms and identify two key insights: 1) Embeddings of subtables exhibit intra-GnR locality, which can be reused multiple times within and beyond a single GnR, and 2) the smallest subtables are compact enough to fit within a bank group.

To leverage these insights, we incorporate an SRAM cache in bg-PIM to prefetch high locality embeddings before GnR execution. To reduce CPU-PIM communication overhead, we propose a subtable mapping strategy that duplicates selected subtables across bank groups. ProactivePIM can be applied for various memory-intensive workloads with skewed data access patterns and operations such as GnR or aggregation [31]. This includes applications like PageRank [7] and the original DLRM, taking advantage of its cache and 2-level PIM architecture. The key contributions of our work are as follows:

- We propose ProactivePIM, a specialized memory architecture for weight-sharing algorithms. To our knowledge, ProactivePIM is the first to address model size reduction.
- We conduct a detailed analysis of weight-sharing algorithms, identifying its drawbacks and intra-GnR locality.
- We provide an efficient prefetching scheme and subtable mapping strategy to leverage intra-GnR locality and to eliminate CPU-PIM communication overhead.

II. BACKGROUND

A. Challenges in Recommendation System Inference

Industry-scale DLRM implementations reach sizes up to tens of terabytes, sometimes surpassing the maximum memory capacity budget of a single-node inference server. Given that the model quality is closely linked to the size of embedding tables [1], [32], its scale is growing year by year [1], [5], [24]. However, the practical utilization of such large models is constrained by capacity limitations in the server. Furthermore, memory-intensive characteristics limit inference throughput. The sparse feature exhibits irregular and sparse memory access, making it challenging for the embedding layer to benefit from the on-chip memory, coupled with the embedding table size that surpasses the cache capacity. Therefore, the embedding layer necessitates frequent access to the off-chip memory system. As the embedding layer execution takes longer latency than the bottom MLP [11], the memory-bound nature of the embedding layer degrades the inference throughput.

B. NMP/PIM Designs for Recommendation System

Recent studies have integrated NMP/PIM units within DIMMs to accelerate the memory-intensive GnR operations. TensorDIMM [13] and RecNMP [12] have exploited rank-level NMP, whereas TRiM [22] leveraged bankgroup-level PIM. These units perform partial GnR on the data allocated within its node and transfer the result to the host. For embedding placement within memory, horizontal partitioning (HP) stores each embedding in a single memory node but suffers from load imbalance due to sparse, irregular access patterns. In contrast, TensorDIMM utilized vertical partitioning (VP), dividing an embedding across multiple ranks. VP is robust to the load imbalance but comes at the cost of energy inefficiency as concurrent row activations are incurred among multiple ranks. In pursuit of further speedup, the designs mentioned above leveraged the long-tail distribution of embeddings [11],

[12] by placing a dynamic cache inside each NMP or introducing a load-balancing technique [12], [22]. SPACE enhanced throughput and power efficiency using HBM as a static DRAM cache for DIMM, storing frequently accessed embeddings and partial sums [11].

III. ANALYSIS OF WEIGHT-SHARING ALGORITHMS

A. Weight-sharing Algorithms for Embedding Table Reduction

Weight-sharing algorithms, QR-trick [25] and TT-Rec [30], improve compression ratios and mitigate the accuracy loss of the hashing trick [28]. Weight-sharing algorithms transform an embedding table into several *subtables* consisting of *subembeddings*. Therefore, they require an additional reconstruction process before the GnR. This reconstruction, termed collect-and-reconst (CnR) in this paper, involves vector multiplication or GEMV operations.

QR-trick. The QR-trick uses double hashing with quotient and remainder hash functions to generate two subtables: the Q subtable and the R subtable, as shown in Figure 2 (a). The Q subtable maps consecutive original embeddings to the same subembedding based on identical quotient values, while the R subtable maps embeddings separated by the collision value based on identical remainder values. The R subtable size is negligible compared to the Q subtable, as it equals the hash collision value. During inference, the embedding layer reconstructs the original embedding from the subtables. Each hash function processes an input index to generate Q and R subtable indices for retrieving subembeddings. A mathematical operation is then performed on these subembeddings to reconstruct the embedding, where this paper focuses on element-wise vector multiplication, which generally outperforms across various models [25].

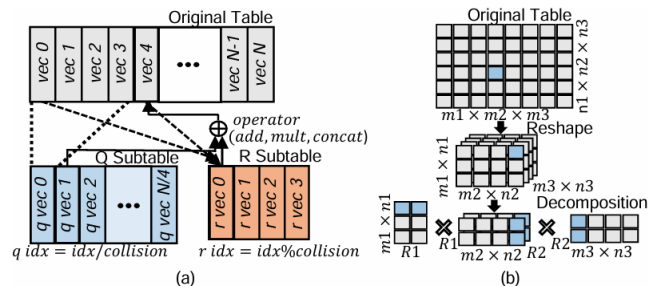


Fig. 2: Weight-sharing algorithms. (a) QR trick with hash collision set to 4 (b) TT-Rec with total TT cores set to 3.

TT-Rec. TT-Rec compresses embedding tables by decomposing them into tensor-train cores (TT-cores) through reshaping and decomposition, as shown in Figure 2 (b). The embedding table $T \in \mathbb{R}^{M \times N}$ is reshaped by factorizing M and N into $M = m_1 \times m_2 \times \dots \times m_d$ and $N = n_1 \times n_2 \times \dots \times n_d$, resulting in $T \in \mathbb{R}^{(m_1 \times n_1) \times (m_2 \times n_2) \times \dots \times (m_d \times n_d)}$. Decomposition then converts the reshaped table into TT-cores, where k th TT-core shape is $C(k) = \mathbb{R}^{R_{k-1} \times (m_k \times n_k) \times R_k}$, $0 < k < d$, where R being the rank and d the number of cores. The rank values are typically set to 16, 32, and 64 and total TT-cores to 3. Note that the TT-cores correspond to subtables in this work.

The second subtable is three-dimensional; each entry consists of R vectors. Reconstructing a full embedding is accomplished by fetching n_1 , n_2 , and n_3 consecutive subembeddings from each subtable and then performing the GEMV followed by a dot product. TT-Rec results in a $327\times$ reduction with the number of subtables and the rank value set to 3 and 32 [30].

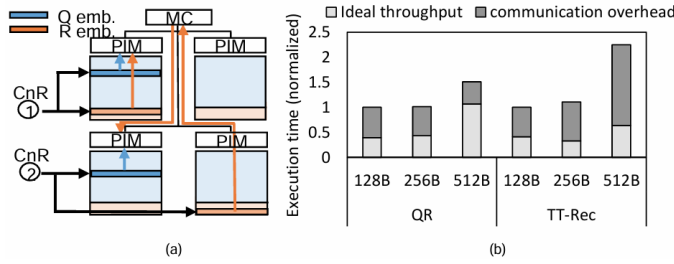


Fig. 3: CPU-PIM communication overview. (a) CPU-PIM communication example (b) Execution time breakdown.

B. Weight-Sharing Algorithms on Previous PIM Systems

The weight-sharing algorithm involves vector multiplication or GEMV operations in the embedding layer for CnR, which require vector pairs to reside in the same PIM unit for computation. However, it is impossible to co-locate all vector pairs within the same node because the subtables are distributed across multiple nodes (e.g., ranks, bank groups) for parallel processing. This requires CPU-PIM communication, as depicted in Figure 3 (a). The second CnR requires the memory controller to pass an operand in a different node. A similar incident occurs for the TT-Rec. Furthermore, as shown in Figure 3 (b), communication overhead takes more than 30% of the total execution time of the embedding layer for all embedding dimensions. Dynamic techniques to alleviate CPU-NMP communication, such as inter-node broadcast [27], face challenges with weight-sharing algorithms. The asynchronous nature of PIM operations for the embedding layer requires each PIM to fetch distinct data, resulting in idle cycles as PIM should wait for data over the shared bus. Although interconnect methods for DIMM-NMP [34] have been proposed to address point-to-point communication, modern PIM architectures still lack support for inter-PIM communication [10]. Even without communication, weight-sharing algorithms incur increased memory access as CnR requires access to all subtables. The abovementioned problems undermine the performance of prior PIM architectures. However, our roofline analysis [29] in Figure 4 shows that both algorithms are within the memory-bound region, indicating that PIM is still a promising solution for embedding layer with weight-sharing algorithms.

C. Access Patterns and Table Characteristics

Each subtable must be accessed concurrently in weight-sharing algorithms to reconstruct an original embedding. The total number of accesses is not distributed but remains the same for each subtable. In addition, the total subembeddings in a subtable are much smaller than the original embedding table. Thus, access to each subembedding becomes more concentrated than the original, intensifying the access rate.

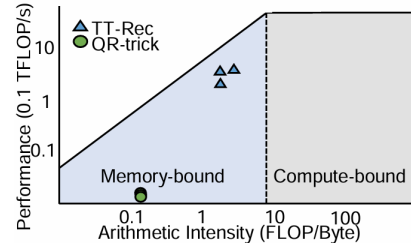


Fig. 4: Roofline analysis. (Evaluated on NVIDIA Tesla V100 with varying batch sizes and total embeddings per GnR.)

Another observation is that subembeddings are reused not only across GnRs of the same batch but also within a single GnR. In conventional recommendation systems, a user’s interaction with an item is typically reflected once in one sparse feature, preventing multiple accesses within a single GnR. However, weight-sharing algorithms map multiple embeddings to a single subembedding, necessitating a CnR before the GnR, thus enabling the reuse of subembeddings. We term this characteristic as intra-GnR locality. As shown in Figure 2 (b), access to consecutive embeddings cause multiple access to the single subembedding within the Q subtable. The intra-GnR locality is further strengthened for smaller subtable sizes, given that access to the subembeddings gets more concentrated. Previous designs are not optimized for such characteristics, losing an opportunity for extra speedup.

IV. PROACTIVEPIM ARCHITECTURE

We propose the ProactivePIM, a PIM architecture that supports weight-sharing algorithm. ProactivePIM employs an integrated approach for speedup by utilizing in-memory cache (detailed in Section IV-B), eliminating communication overhead through data mapping (detailed in Section IV-C), and minimizing additional overhead in the PIM system.

A. ProactivePIM Architecture

Architecture Overview. The overall architecture is depicted in Figure 5 (a). From a top-level view, the ProactivePIM system utilizes a heterogeneous memory architecture comprising multiple HBM stacks and DIMMs. By leveraging the long-tail phenomenon that still exists in weight-sharing algorithms, frequently accessed subembeddings are offloaded to HBM. DIMMs reduce the burden of high compression rates to fit all data into HBM, enabling scalable model inference.

A two-level PIM system is used inside HBM to leverage in-memory parallelism. In Figure 5 (b), the first-level processing unit (bd-PIM) is on the base die, while the second-level units (bg-PIM) are inside each bank group. Each bg-PIM performs CnR followed by GnR on the CnR outputs and passes the partial results to the bd-PIM for final reduction. Figure 5 (d) shows bg-PIM, where PIM instructions (PIM-Inst) delivered from the host are buffered and then decoded in the decoder to set control paths of the PIM unit. Memory-mapped register (MMReg) is placed within the decoder to indicate the prefetch address’s start and end. MAC unit performs CnR/GnR, while prefetched subembeddings are stored inside the cache to utilize

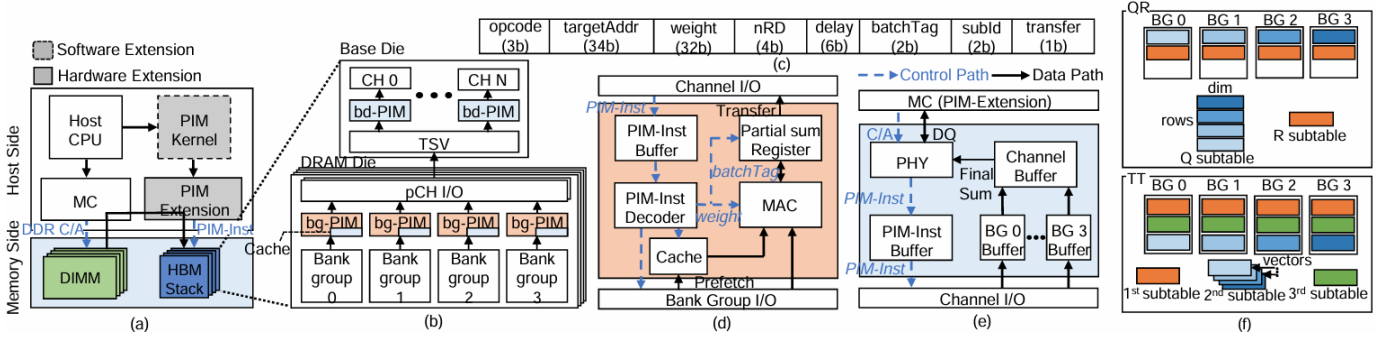


Fig. 5: Overview. (a) ProactivePIM architecture (b) 2-level PIM system (c) PIM instruction (d) bg-PIM (e) bd-PIM (f) Subtable mapping for QR-trick/TT-Rec.

intra-GnR locality. The HP method is employed for data placement, as its energy efficiency is better than VP’s. Figure 5 (e) shows bd-PIM, similar to the bg-PIM without the cache and MAC unit. The architecture can also support original DLRM or PageRank [7], leveraging cache to store feature vectors of frequently accessed vertices for higher throughput [31].

Execution Flow. Like prior works [12], [22], the PIM kernel launched by the host CPU sends PIM requests to the memory controller extension (PIM extension), which schedules and issues PIM-Inst to start CnR/GnR. If the subembeddings are in the DIMM, they are read by the memory controller, passed through the PIM extension, and packed into the PIM-Inst. To handle the C/A bandwidth overhead [22], we follow prior methods that utilize DQ pins to deliver PIM-Inst to bg-PIMs within a short cycle. We use direct mapping method to support PIM operations and allocate memory space for ProactivePIM as uncachable to avoid the cache coherence. The support for heterogeneous memory has been covered in previous research [11]. Thus, they will not be discussed in detail here.

PIM Instruction. Figure 5 (c) depicts PIM-Inst format. The *opcode* (3-bit) specifies the operation type that bg-PIM should execute, the *target address* (34-bit) denotes the start address of the data to be read from the node, and the *weight* (32-bit) delivers weight value for weighted sum. The *nRD* (4-bit) indicates the subembedding size, and the *delay* (6-bit) instructs the time for instruction decode after being delivered to the bg-PIM. The *batchTag* (2-bit) is the assigned batch of the instruction, and the *subid* (2-bit) indicates the subtable id, used for CnR termination. Finally, *transfer* (1-bit) determines whether the partial sum is complete and ready to deliver.

B. Hot Subembedding Prefetch

To leverage intra-GnR locality, “hot” subembeddings with high access frequency are cached into bg-PIM before the CnR/GnR execution. During the CnR/GnR, hot subembedding accesses are directed to the cache. Partial sum transfer and prefetching are pipelined to minimize the prefetch overhead, by utilizing separate buses: transfer uses an external bus, while prefetching uses an internal bus, as shown in Figure 5 (d). When PIM-Inst for data transfer is issued from the decoder, bg-PIM starts to prefetch. To ensure correct timing for cached data access, the PIM extension needs to store physical

addresses of cached data for reference. The corresponding area overhead is mitigated by prefetching an entire subtable. As described in Section IV-C, specific subtables are replicated in each bank group; the extension only checks the subtable ID for issuing cached data access as an entire subtable is prefetched.

Target Subtable to Prefetch. The key criteria for selecting a target subtable are (i) the degree of intra-GnR locality and (ii) the subtable size, both of which influence cache efficiency. In the QR-trick, the R subtable is much smaller than the Q subtable, and subembeddings exhibit high intra-GnR locality as described in Section III-A. Therefore, the R subtable is chosen. For TT-Rec, the intra-GnR locality is similar among all the subtables, but the second subtable is three-dimensional, resulting in a larger size. Furthermore, as described in Section IV-C, the subembedding dimension of the third table is smaller than the other tables, which degrades cache efficiency. Therefore, the first subtable is the target.

Prefetch Method. Figure 6 (a) shows the original execution timeline for CnR/GnR execution of three original tables. Once CnR/GnR completes for table A, the partial sums from each bg-PIM are transferred to the bd-PIM during the transfer phase. Figure 6 (b) illustrates the naive method in which all target subtables are read and offloaded before the embedding layer execution, which we name all-table prefetch. At the cost of the initial delay, the time consumed in PIM operation is largely reduced due to the cache hit. This effect is permanent before the inference terminates. However, this method requires a large SRAM cache to store all the target subtables. When there are 20 tables, 17% area overhead in DRAM die occurs, which worsens with more tables. VP could be utilized to reduce SRAM size fourfold by distributing subembedding dimensions across bank groups. However, for dimensions smaller than 256B, the data read per access falls below the DRAM burst granularity, reducing efficiency.

Observing that batches are scheduled table-wise in the embedding layer, ProactivePIM adopts a table-wise prefetch scheme. This approach offloads target subembeddings of the next table once the CnR/GnR of the previous table completes, as illustrated in Figure 6 (c). Before CnR/GnR begins for table B, the target subtable is prefetched to the cache during table A’s data transfer phase, with the same process for tables B and C. This method allows the SRAM cache to accommodate only

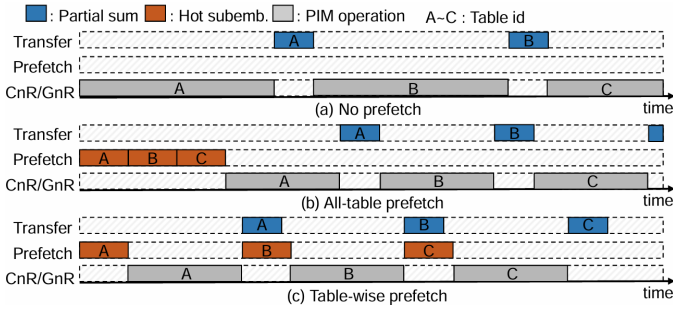


Fig. 6: CnR/GnR execution timeline without and with prefetch.

a single subtable, significantly reducing PIM area overhead.

As shown in equation 1, the transfer latency ($t_{Transfer}$) is proportional to the total bank groups in a channel, read command delay between bank groups (t_{ccd_s}), batch size, and the embedding dimension (v_{len}). In contrast, the prefetch latency ($t_{Prefetch}$) is proportional to total subembeddings within a target subtable (t_{otsub}), read command delay within bank groups (t_{ccd_l}), and subembedding dimension ($subv_{len}$). As a small batch size could cause severe load imbalance across PIM nodes, especially critical for a multi-stack HBM system, we choose a batch size 16. As described in Section VI-D, prefetch overhead is minimal, which indicates $t_{Prefetch}$ is similar to $t_{Transfer}$. The host reads MMRReg in the PIM to verify prefetch completion to enable next CnR/GnR execution. Target subtable data are mapped consecutively in a row to utilize the row buffer hit.

$$t_{Transfer} = batch \times v_{len} \times bankgroups \times t_{ccd_s} \quad (1)$$

$$t_{Prefetch} = t_{otsub} \times subv_{len} \times t_{ccd_l} \quad (2)$$

C. Subtable Mapping Strategy

ProactivePIM devises a subtable mapping strategy to eliminate the CPU-PIM communication. This strategy is based on the observation that the number of entries in each subtable differs significantly. ProactivePIM replicates small subtables into every PIM node so that element-wise multiplication is performed without CPU-PIM communication. As shown in Figure 5 (f), in the QR-trick, the R subtable is duplicated among the bank groups, while in TT-Rec, the 1st and 3rd subtables are duplicated. The remaining subtables in both methods are distributed among the bank groups.

The duplication overhead becomes critical as in-memory parallelism deepens, especially as the number of original tables increases. For example, with a 512B embedding size, the duplication overhead is 12MB for QR-trick (with a hash collision value of 60) and 10MB for TT-Rec (assuming a rank value of 16 and 1600 total subembeddings). At the bank group level, the capacity overhead from duplication is less than 4.7% in HBM2. However, this overhead rises significantly at the bank level, reaching a maximum of 18.8%. To reduce memory capacity overhead, ProactivePIM uses bank group-level PIM.

TT-Rec cannot benefit from the cache when a whole CnR is performed inside a single PIM unit. The first stage of CnR

in TT-Rec is GEMV on the 1st and 2nd subtable, requiring the 3rd subtable subembedding to wait until all the vector multiplication of GEMV is complete. Even when the cache is utilized, the speedup is minimal since the computation start time of the 3rd subtable remains similar. Therefore, as shown in Figure 5 (f), we employ row-wise partitioning, distributing the vectors that form a 2nd subtable subembedding across bank groups. Each PIM performs individual vector multiplications instead of a GEMV operation, enabling the computation on 3rd subtable subembedding to be performed immediately after data is read, where only partial data is used for distributed multiplication. The host handles the final reduction.

During preprocessing, the PIM kernel duplicates specified subtables by sending write commands with the top bit of the physical address set to 1. The PIM extension detects this bit and broadcasts the command to all bank groups. Once duplication is complete, the PIM kernel allocates the remaining subtables to available spaces. During inference, the extension checks the top bit and adjusts the channel and bank group in the PIM-Inst for duplicated subtables.

V. EXPERIMENTAL SETUP

Implementation. We implement ProactivePIM on DRAM-sim3 [15], a cycle-accurate memory simulator. HBM2 \times 128 and DDR4-3200 \times 8 were set to base memory systems, where Table I summarizes the specifications. We compare ProactivePIM performance against RecNMP, TRiM and SPACE. Hot subembeddings are treated as hot embeddings to utilize existing designs that exploit temporal locality. We generate synthetic traces of CnR/GnR from the official DLRM code using criteo datasets [3], [23]. The embedding lookup per GnR is set to 80, with dimensions ranging from 128B to 512B.

TABLE I: Memory System Specification

HBM2 \times 128 device	
Component	1 stack of HBM2 (4GB)
Memory Organization	8 channels per 4-hi stack, 4 bank-groups per channel, 4 banks per bank-group
Timing Parameters	tCL=14, tRP=14, tRCD=14, tCCD_S=1, tCCD_L=2, tBL=4
Clock Frequency	1000MHz
DDR4-3200 \times 8 device	
Component	2 DIMM module (16GB)
Memory Organization	1 channel per DIMM, 2 ranks per channel, 4 bank-groups per rank, 4 banks per bank-group
Timing Parameter	tCL=22, tRP=22, tRCD=22, tCCD_S=4, tCCD_L=8, tBL=8
Clock Frequency	1600MHz

Area Overhead and Power Consumption. Bd-PIM and bg-PIM were synthesized using Synopsys Design Compiler with 45nm CMOS technology operating at 300MHz clock frequency to obtain the area overhead and power consumption. The area was scaled to a 20nm DRAM process, taking into account that the DRAM process is 10 \times less dense compared to ASIC process [4]. The SRAM cache power was estimated using CACTI 6.5 [18]. The power consumption of memory was calculated following [20].

VI. EVALUATION RESULTS

As the first step in analyzing ProactivePIM’s effectiveness, we evaluate the impact of each proposed method. We then compare ProactivePIM’s performance on GnR with prior NMP designs. The cache size is set to the largest target subtable size of QR-trick and TT-Rec, 100KB.

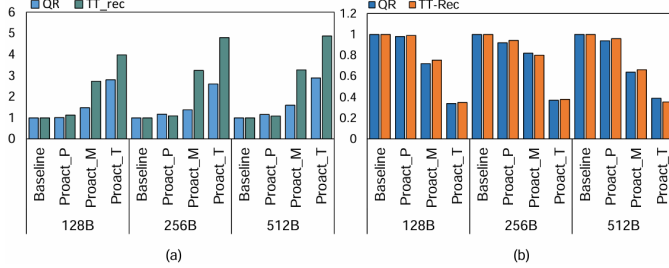


Fig. 7: Performance of design choices on QR-trick/TT-Rec. (a) Relative speedup (b) Relative energy consumption. Results are normalized to the baseline.

A. Performance Impact of Design Optimizations

We evaluate the impact of our design choices on the speedup. Figure 7 shows speedup and energy efficiency improvements as design optimizations are incrementally applied to the ProactivePIM system. The baseline is normal HBM2 with the last-level cache of the host set to 32MB. The first two configurations, Proact_P and Proact_M, are PIM systems without SRAM cache: Proact_P adds only bg-PIM to the baseline, while Proact_M applies the subtable mapping strategy on Proact_P. Finally, Proact_T represents our complete PIM system with table-wise prefetch. With a 512B embedding size, Proact_P and Proact_M achieve speedups of a 8% and 69% for QR-trick, and 13% and 272% for TT-Rec, respectively. The performance of Proact_P is lower than the ideal speedup target of $2\times$ (bank groups \times tccd_s/tccd_l) in HBM2, caused by the CPU-PIM communication overhead. Proact_M achieves 39% performance improvement than Proact_P by eliminating the overhead, also reducing energy consumption by 32%. In each algorithm, Proact_T achieves $2.84\times$ and $4.8\times$ better results than the baseline, leveraging SRAM cache for intra-GnR locality. Proact_T outperforms in energy efficiency due to decreased activation and read energy. Prefetch overhead is minimal as speedup of Proact_T over Proact_M is nearly ideal.

B. Performance Evaluation with Previous NMP Designs

We evaluate ProactivePIM’s throughput against prior PIM systems, RecNMP, TRiM-G, and SPACE, using HBM2 as the base memory architecture with a consistent subtable mapping strategy for fair comparison. TensorDIMM is excluded as its configuration in HBM2 results in inefficient memory access below the granularity threshold. Figure 8 (a) shows the relative speedup of each previous work normalized to the RecNMP for each algorithm, where embedding size ranges from 128B to 512B. When 512B embedding size, Proact_T achieves $4\times$,

$4.7\times$, $4.9\times$ speedup compared to each configuration in TT-Rec. The result is similar to the QR trick. ProactivePIM’s achievement comes from efficient cache utilization by leveraging intra-GnR locality and subtable mapping strategy. The impact gets more significant for large dimensions due to increased data reads per bg-PIM.

Figure 8 (b) depicts the relative energy consumption of prior works and ProactivePIM, which are normalized to the result of RecNMP. To properly measure the energy efficiency of the HBM-DIMM architecture over DIMM, two DIMMs are utilized across systems. Energy consumption is saved 54.1%, 53%, and 52% compared to RecNMP, TRiM-G and SPACE when mapping strategy is applied. The energy efficiency comes from the decreased access due to SRAM cache, along with the reduction in static energy from shorter inference time.

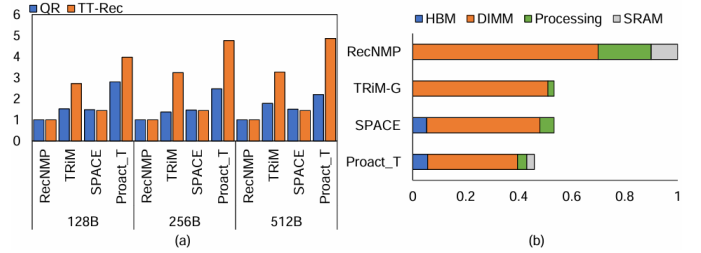


Fig. 8: Performance evaluation of QR-trick/TT-rec on NMP/PIM systems. (a) Speedup comparison (b) Energy consumption breakdown for QR-trick.

C. Sensitivity Study of Cache Capacity

We conduct a sensitivity study on the cache capacity to prove the necessity of the table-wise prefetch method for SRAM size reduction and to show that SRAM overhead is minimal in such method. As all-table prefetch stores all the target subtables, the area overhead gets larger as more embedding tables are employed. Figure 9 shows variation in PIM area overhead when the total embedding table increases. When the total table is 20, the area overhead of PIM on HBM2 die is nearly 17% in QR-trick and 15% in TT-Rec.

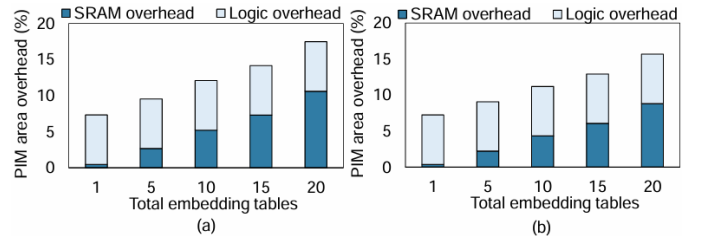


Fig. 9: SRAM cache sensitivity study. (a) QR-trick (b) TT-Rec

D. Design Overhead

The total area occupied by bg-PIM is $6.58mm^2$ per HBM2 die, taking a 6.8% area overhead. SRAM cache takes 7% of the total PIM area. The total gate count is 125,740 per bg-PIM, where each PIM includes eight MAC units, registers, and logic support. The area overhead of bd-PIM is $1.63mm^2$ per channel, with a gate count of 118,087 each.

VII. CONCLUSION

We propose ProactivePIM, a two-level PIM architecture that accelerates weight-sharing algorithms by leveraging intra-GnR locality and subtable duplication. We analyzed weight-sharing algorithm characteristics and defined CPU-PIM communication overhead issues and intra-GnR locality. By incorporating an SRAM cache within the bg-PIM and implementing an efficient prefetch strategy with subtable mapping, ProactivePIM enhances CnR/GnR throughput. This results in a $4.8\times$ performance improvement compared to previous architectures.

REFERENCES

- [1] Ehsan K Ardestani, Changkyu Kim, Seung Jae Lee, Luoshang Pan, Jens Axboe, Valmiki Rampersad, Banit Agrawal, Fuxun Yu, Ansha Yu, Trung Le, et al. Supporting massive dlrn inference through software defined memory. In *2022 IEEE 42nd International Conference on Distributed Computing Systems (ICDCS)*, pages 302–312. IEEE, 2022.
- [2] Paul Covington, Jay Adams, and Emre Sargin. Deep neural networks for youtube recommendations. In *Proceedings of the 10th ACM conference on recommender systems*, pages 191–198, 2016.
- [3] CriteoLabs. 2014. Kaggle display advertising challenge dataset. [Online]. Available : <https://jmcauley.ucsd.edu/data/amazon/>.
- [4] Fabrice Devaux. The true processing in memory accelerator. In *2019 IEEE Hot Chips 31 Symposium (HCS)*, pages 1–24. IEEE Computer Society, 2019.
- [5] Amin Firoozshahian, Joel Coburn, Roman Levenstein, Rakesh Nattoji, Ashwin Kamath, Olivia Wu, Gurdeepak Grewal, Harish Aepala, Bhasker Jakka, Bob Dreyer, et al. Mtia: First generation silicon targeting meta’s recommendation systems. In *Proceedings of the 50th Annual International Symposium on Computer Architecture*, pages 1–13, 2023.
- [6] Antonio A Ginart, Maxim Naumov, Dheevatsa Mudigere, Jiyan Yang, and James Zou. Mixed dimension embeddings with application to memory-efficient recommendation systems. In *2021 IEEE International Symposium on Information Theory (ISIT)*, pages 2786–2791. IEEE, 2021.
- [7] Joseph E Gonzalez, Yucheng Low, Haijie Gu, Danny Bickson, and Carlos Guestrin. {PowerGraph}: Distributed {Graph-Parallel} computation on natural graphs. In *10th USENIX symposium on operating systems design and implementation (OSDI 12)*, pages 17–30, 2012.
- [8] Udit Gupta, Carole-Jean Wu, Xiaodong Wang, Maxim Naumov, Brandon Reagen, David Brooks, Bradford Cottel, Kim Hazelwood, Mark Hempstead, Bill Jia, et al. The architectural implications of facebook’s dnn-based personalized recommendation. In *2020 IEEE International Symposium on High Performance Computer Architecture (HPCA)*, pages 488–501. IEEE, 2020.
- [9] Mingxuan He, Choungki Song, Ilkon Kim, Chunseok Jeong, Seho Kim, Il Park, Mithuna Thottethodi, and TN Vijaykumar. Newton: A dram-maker’s accelerator-in-memory (aim) architecture for machine learning. In *2020 53rd Annual IEEE/ACM International Symposium on Microarchitecture (MICRO)*, pages 372–385. IEEE, 2020.
- [10] Gilbert Jonatan, Haeyoon Cho, Hyojun Son, Xiangyu Wu, Neal Livesay, Evelio Mora, Kaustubh Shivdikar, José L Abellán, Ajay Joshi, David Kaeli, et al. Scalability limitations of processing-in-memory using real system evaluations. *Proceedings of the ACM on Measurement and Analysis of Computing Systems*, 8(1):1–28, 2024.
- [11] Hongju Kal, Seokmin Lee, Gun Ko, and Won Woo Ro. Space: locality-aware processing in heterogeneous memory for personalized recommendations. In *2021 ACM/IEEE 48th Annual International Symposium on Computer Architecture (ISCA)*, pages 679–691. IEEE, 2021.
- [12] Liu Ke, Udit Gupta, Benjamin Youngjae Cho, David Brooks, Vikas Chandra, Utku Diril, Amin Firoozshahian, Kim Hazelwood, Bill Jia, Hsien-Hsin S Lee, et al. Recnmp: Accelerating personalized recommendation with near-memory processing. In *2020 ACM/IEEE 47th Annual International Symposium on Computer Architecture (ISCA)*, pages 790–803. IEEE, 2020.
- [13] Youngeun Kwon, Yunjae Lee, and Minsoo Rhu. Tensordimm: A practical near-memory processing architecture for embeddings and tensor operations in deep learning. In *Proceedings of the 52nd Annual IEEE/ACM International Symposium on Microarchitecture*, pages 740–753, 2019.
- [14] Sukhan Lee, Shin-haeng Kang, Jaehoon Lee, Hyeonsu Kim, Eojin Lee, Seungwoo Seo, Hosang Yoon, Seungwon Lee, Kyoungwan Lim, Hyunsung Shin, et al. Hardware architecture and software stack for pim based on commercial dram technology: Industrial product. In *2021 ACM/IEEE 48th Annual International Symposium on Computer Architecture (ISCA)*, pages 43–56. IEEE, 2021.
- [15] Shang Li, Zhiyuan Yang, Dhiraj Reddy, Ankur Srivastava, and Bruce Jacob. Dramsim3: A cycle-accurate, thermal-capable dram simulator. *IEEE Computer Architecture Letters*, 19(2):106–109, 2020.
- [16] Fuyuan Lyu, Xing Tang, Hong Zhu, Huifeng Guo, Yingxue Zhang, Ruiming Tang, and Xue Liu. Optembed: Learning optimal embedding table for click-through rate prediction. In *Proceedings of the 31st ACM International Conference on Information & Knowledge Management*, pages 1399–1409, 2022.
- [17] Dheevatsa Mudigere, Yuchen Hao, Jianyu Huang, Zhihao Jia, Andrew Tulloch, Srinivas Sridharan, Xing Liu, Mustafa Ozdal, Jade Nie, Jongsoo Park, et al. Software-hardware co-design for fast and scalable training of deep learning recommendation models. In *Proceedings of the 49th Annual International Symposium on Computer Architecture*, pages 993–1011, 2022.
- [18] Naveen Muralimanohar, Rajeev Balasubramonian, and Norman P Jouppi. Cacti 6.0: A tool to model large caches. *HP laboratories*, 27:28, 2009.
- [19] Maxim Naumov, Dheevatsa Mudigere, Hao-Jun Michael Shi, Jianyu Huang, Narayanan Sundaraman, Jongsoo Park, Xiaodong Wang, Udit Gupta, Carole-Jean Wu, Alisson G Azzolini, et al. Deep learning recommendation model for personalization and recommendation systems. *arXiv preprint arXiv:1906.00091*, 2019.
- [20] Mike O’Connor, Niladrish Chatterjee, Donghyuk Lee, John Wilson, Aditya Agrawal, Stephen W Keckler, and William J Dally. Fine-grained dram: Energy-efficient dram for extreme bandwidth systems. In *Proceedings of the 50th Annual IEEE/ACM International Symposium on Microarchitecture*, pages 41–54, 2017.
- [21] Jaehyun Park, Jaewan Choi, Kwanhee Kyung, Michael Jaemin Kim, Yongsuk Kwon, Nam Sung Kim, and Jung Ho Ahn. Attacc! unleashing the power of pim for batched transformer-based generative model inference. In *Proceedings of the 29th ACM International Conference on Architectural Support for Programming Languages and Operating Systems, Volume 2*, pages 103–119, 2024.
- [22] Jaehyun Park, Byeongho Kim, Sungmin Yun, Eojin Lee, Minsoo Rhu, and Jung Ho Ahn. Trim: Enhancing processor-memory interfaces with scalable tensor reduction in memory. In *MICRO-54: 54th Annual IEEE/ACM International Symposium on Microarchitecture*, pages 268–281, 2021.
- [23] Vijay Janapa Reddi, Christine Cheng, David Kanter, Peter Mattson, Guenther Schmuelling, Carole-Jean Wu, Brian Anderson, Maximilien Breughe, Mark Charlebois, William Chou, et al. Mlperf inference benchmark. In *2020 ACM/IEEE 47th Annual International Symposium on Computer Architecture (ISCA)*, pages 446–459. IEEE, 2020.
- [24] Geet Sethi, Bilge Acun, Niket Agarwal, Christos Kozyrakis, Caroline Trippel, and Carole-Jean Wu. Recsharp: statistical feature-based memory optimization for industry-scale neural recommendation. In *Proceedings of the 27th ACM International Conference on Architectural Support for Programming Languages and Operating Systems*, pages 344–358, 2022.
- [25] Hao-Jun Michael Shi, Dheevatsa Mudigere, Maxim Naumov, and Jiyan Yang. Compositional embeddings using complementary partitions for memory-efficient recommendation systems. In *Proceedings of the 26th ACM SIGKDD International Conference on Knowledge Discovery & Data Mining*, pages 165–175, 2020.
- [26] Harald Steck, Linas Baltrunas, Ehtsham Elahi, Dawen Liang, Yves Raimond, and Justin Basilico. Deep learning for recommender systems: A netflix case study. *AI Magazine*, 42(3):7–18, 2021.
- [27] Weiye Sun, Zhaoshi Li, Shouyi Yin, Shaojun Wei, and Leibo Liu. Abcdimm: Alleviating the bottleneck of communication in dimm-based near-memory processing with inter-dimm broadcast. In *2021 ACM/IEEE 48th Annual International Symposium on Computer Architecture (ISCA)*, pages 237–250. IEEE, 2021.
- [28] Kilian Weinberger, Anirban Dasgupta, John Langford, Alex Smola, and Josh Attenberg. Feature hashing for large scale multitask learning. In *Proceedings of the 26th annual international conference on machine learning*, pages 1113–1120, 2009.
- [29] Samuel Williams, Andrew Waterman, and David Patterson. Roofline: an insightful visual performance model for multicore architectures. *Communications of the ACM*, 52(4):65–76, 2009.

- [30] Chunxing Yin, Bilge Acun, Carole-Jean Wu, and Xing Liu. Tt-rec: Tensor train compression for deep learning recommendation models. *Proceedings of Machine Learning and Systems*, 3:448–462, 2021.
- [31] Sungmin Yun, Byeongho Kim, Jaehyun Park, Hwayong Nam, Jung Ho Ahn, and Eojin Lee. Grande: Near-data processing architecture with adaptive matrix mapping for graph convolutional networks. *IEEE Computer Architecture Letters*, 21(2):45–48, 2022.
- [32] Mark Zhao, Niket Agarwal, Aarti Basant, Buğra Gedik, Satadru Pan, Mustafa Ozdal, Rakesh Komuravelli, Jerry Pan, Tianshu Bao, Haowei Lu, et al. Understanding data storage and ingestion for large-scale deep recommendation model training: Industrial product. In *Proceedings of the 49th Annual International Symposium on Computer Architecture*, pages 1042–1057, 2022.
- [33] Weijie Zhao, Jingyuan Zhang, Deping Xie, Yulei Qian, Ronglai Jia, and Ping Li. Aibox: Ctr prediction model training on a single node. In *Proceedings of the 28th ACM International Conference on Information and Knowledge Management*, pages 319–328, 2019.
- [34] Zhe Zhou, Cong Li, Fan Yang, and Guangyu Sun. Dimm-link: Enabling efficient inter-dimm communication for near-memory processing. In *2023 IEEE International Symposium on High-Performance Computer Architecture (HPCA)*, pages 302–316. IEEE, 2023.